Coastal polynyas enable transitions between high and low West Antarctic ice shelf melt rates

Ruth Moorman[1], Andrew F. Thompson[1], and Earle A. Wilson[2]

[1]Environmental Science and Engineering, California Institute of Technology, Pasadena, California, USA
[2]Department of Earth System Science, Stanford University, Stanford, California, USA

Key Points:

- Rates of ocean-driven Amundsen Sea ice shelf melt respond to variations in warm water transport to the coast and modification at the coast.
- A simple Amundsen Sea continental shelf overturning model, based on water mass transformation, reveals bistable high and low melt regimes.
- Feedbacks between glacial melt and polynya convection are central to the bistability and produce variability consistent with observations.

Corresponding author: Ruth Moorman, rmoorman@caltech.edu

Abstract

Melt rates of West Antarctic ice shelves in the Amundsen Sea track large decadal variations in the volume of warm water at their outlets. This variability is generally attributed to wind-driven variations in warm water transport towards ice shelves. Inspired by conceptual representations of the global overturning circulation, we introduce a simple model for the evolution of the thermocline, which caps the water warm layer at the ice-shelf front. This model demonstrates that interannual variations in coastal polynya buoyancy forcing can generate large decadal-scale thermocline depth variations, even when the supply of warm water from the shelf-break is fixed. The modeled variability involves transitions between bistable high and low melt regimes, enabled by feedbacks between basal melt rates and ice front stratification strength. Our simple model captures observed variations in near-coast thermocline depth and stratification strength, and poses an alternative mechanism for warm water volume changes to wind-driven theories.

Plain Language Summary

Ice loss from the West Antarctic Ice Sheet contributes significantly to current rates of global sea-level rise and threatens to raise sea-levels by 5 m should it collapse completely. The ice sheet is primarily losing mass via glaciers that flow from the Antarctic continent into the Amundsen Sea, where floating ice shelves are exposed to much warmer ocean waters than elsewhere around Antarctica. In this work we present a simplified mathematical model for the volume of warm water at Amundsen Sea ice shelf fronts that successfully reproduces observed patterns of warm water variability. The modeled variability relies on interactions between ice shelf melt and coastal polynyas, regions where enhanced wintertime sea-ice production can trigger mixing that diverts heat carried by warm waters away from the ice shelf and into the atmosphere. Higher melt rates inhibit polynya convection, allowing more warm water to access the ice shelf cavity and reinforcing a high melt state, whilst lower melt rates facilitate polynya convection, diverting heat away from the ice shelf and reinforcing a low melt state. Our results promote the importance of coastal processes in explaining observed variations in Amundsen Sea ice shelf melt, which have previously been attributed to remote wind patterns.

1 Introduction

Recorded mass loss from the West Antarctic Ice Sheet (WAIS) has been driven by the accelerating flow of ice streams that terminate at rapidly thinning ice shelves in the Amundsen Sea embayment (Mouginot et al., 2014; Paolo et al., 2015; IMBIE Team, 2018). These ice streams drain a land ice catchment containing a potential ∼1.2 m of sea level rise (Fretwell et al., 2013). Whilst ice shelf thinning does not directly impact the ice sheet mass balance, the restraining or "buttressing" effect of floating ice shelves on upstream grounded ice flow is critical for limiting ice discharge through glaciers (Fürst et al., 2016; Morlighem et al., 2020). The observed thinning of buttressing ice shelves in the Amundsen Sea has been associated with high rates of basal melt driven by modified Circumpolar Deep Water (mCDW) (Adusumilli et al., 2020; Pritchard et al., 2012; Shepherd et al., 2004; Turner et al., 2017); a warm (2-4°C above freezing) water mass that floods the lower layers of the West Antarctic continental shelf and carries heat from the open ocean to ice shelf cavities via glacially-carved troughs (Walker et al., 2007; Dutrieux et al., 2014). Future projections of the WAIS require accurate representation of forcings that dictate the access of warm mCDW to Amundsen Sea ice shelf cavities.

Hydrographic observations from the Amundsen Sea embayment reveal decadal variations in the thickness of the mCDW layer (Dutrieux et al., 2014; Jenkins et al., 2018) that overwhelm multidecadal ocean warming trends previously considered the driver of ice shelf thinning (Schmidtko et al., 2014). This decadal variability is well observed in front of the Dotson Ice Shelf (Figure 1a), a rapidly thinning shelf buttressing the Kohler

and Smith glaciers (Paolo et al., 2015). Here, the Amundsen Sea Polynya (ASP) permits the repeated collection of summertime hydrographic profiles along the ice shelf front between 2000 and 2018 (Figure 1). These observations reveal high amplitude ($\sim$ 400 m), low frequency ($\sim$ 10 year period) variability in the thermocline depth, characterized by a warm phase with thick mCDW from 2006-2011 followed by a cool phase with thin mCDW from 2012-2016 and a potential return to warm conditions in 2018 (Figure 1b,d) (Jenkins et al., 2018; Kim et al., 2021). The observed thermocline variability has been linked to Dotson Ice Shelf basal melt rates (Jenkins et al., 2018) and may be implicated in ice shelf thinning trends, either via historical warm phases triggering geometric grounding line retreat that continues to the present (Jenkins et al., 2016) or via a trend in the frequency of warm phases unresolved by the short observational record (Naughten et al., 2022).

Though past studies have shown correlations between shoreward mCDW transport and wind forcing over the shelf-break, the mechanistic link between these processes remains uncertain. Studies focused on monthly to interannual timescales suggest eastward wind anomalies over the shelf enhance mCDW transport through troughs via barotropic acceleration of the Amundsen undercurrent (Assmann et al., 2013; Dotto et al., 2019, 2020; Naughten et al., 2022) and localized shelf-break (Kim et al., 2017; Webber et al., 2019) or shelf integrated (Kim et al., 2021) Ekman pumping. By contrast, Silvano et al. (2022) find the opposite relation at decadal timescales, an anticorrelation between eastward wind anomalies and shoreward mCDW transport, due to baroclinic adjustment of the Amundsen undercurrent. Though proposed mechanisms differ, these studies consistently present wind-driven variability of shoreward mCDW transport as the driver of decadal thermocline depth variability and related melt variability in the Amundsen sector.

There are indications that the wind-driven framework is incomplete. Coastal thermocline depth and heat content variability is substantially amplified relative to the shelf-break in both observations and simulations (e.g. Kim et al., 2021; Silvano et al., 2022; Naughten et al., 2022), a feature not yet explained by wind-driven mechanisms. Further, while thermocline displacements predicted from winds correlate well with observations, they underestimate the amplitude of coastal signals (Kim et al., 2021). Prompted by this amplitude gap, we revisit the Dotson Ice Front hydrography. Years with thick mCDW layers (2006-2011) are consistently associated with stronger stratification (Figure 1d) and more buoyant, meltwater modified Winter Waters (WW) relative to years with thin mCDW layers (2000, 2012-2016). Further, during warm years, modification by glacial meltwater pulls WW, a remnant of the preceding winter's sea-ice modified mixed layer, away from the freezing line and towards the mCDW-meltwater mixing line (the "Gade Line") (Figure 1c). These hydrographic properties suggest an underappreciated role for water mass transformation by sea-ice and glacial ice in the observed variability.

Informed by a high-resolution regional ocean simulation and the observations presented above, we introduce a simple overturning circulation model that represents the transformation of mCDW into cool thermocline waters both within the Dotson Ice Shelf cavity and at its entrance in the ASP. Using this model, we demonstrate that variations in polynya surface buoyancy fluxes, directly related to net local sea-ice formation rates, can generate large decadal scale thermocline depth variations in the absence of variable shelf-break forcing, posing an alternative mechanism for observed variability. The modeled thermocline variability takes the form of transitions between bistable warm and cool regimes, made possible by feedbacks between basal ice melt and stratification at the ice front. With this work, we underscore that variations in mCDW consumption, in addition to mCDW supply, can strongly influence the exposure of West Antarctic ice shelves to ocean heat. This work uses the Dotson Ice Shelf as a case study, however our model is applicable to other West Antarctic ice shelves fringed by coastal polynyas, including Venable and Pine Island ice shelves.

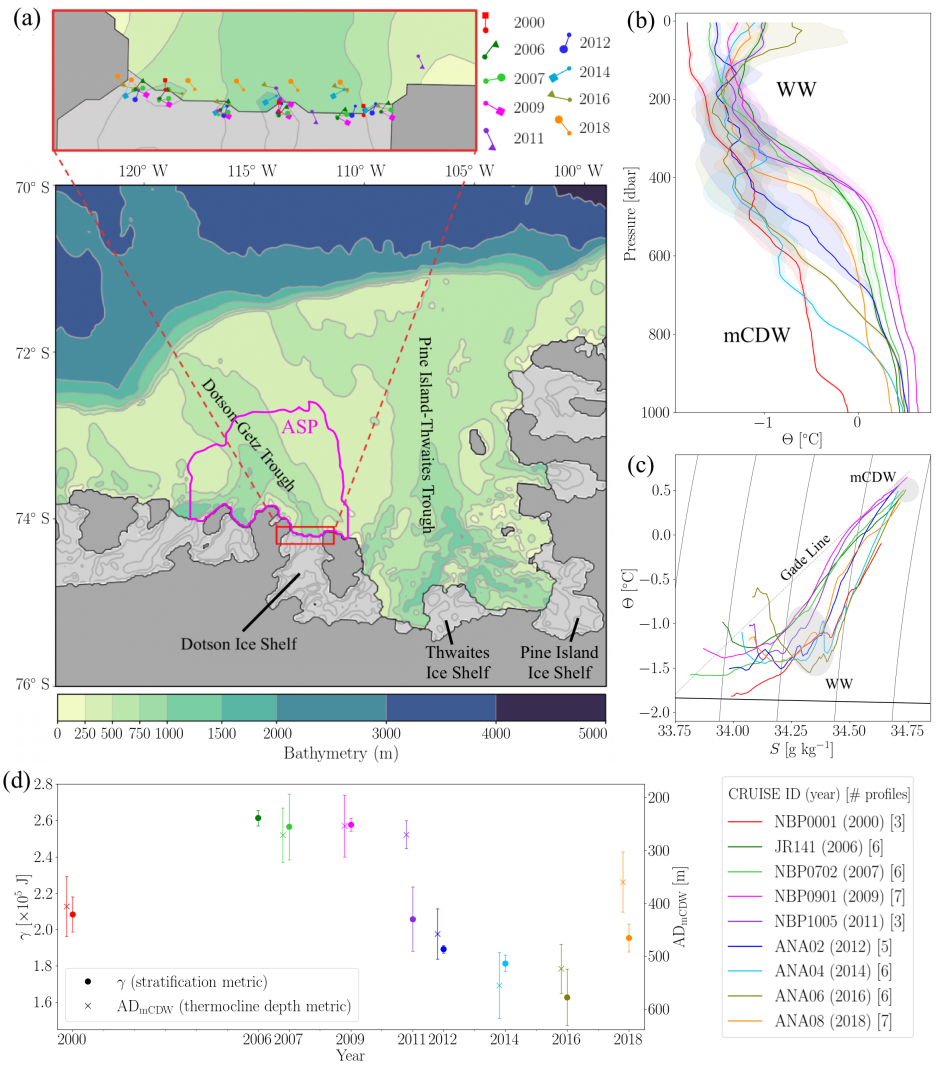

Figure 1. (a) Map of the Amundsen Sea embayment showing open ocean bathymetry (green shading; grey contours), ice shelf cavity bathymetry (grey shading; grey contours), and the grounded ice zone (dark grey). The Dotson Ice Front is outlined in red with an enlarged view provided above. The January climatological mean (2004-2022) extent of the Amundsen Sea Polynya (ASP) is indicated by the pink contour (using Fetterer & Stewart., 2020). Locations of shipborne observations used to produce (b)-(d) are indicated in the enlarged map. (b,c) Cruise mean conservative temperature (Θ) profiles as a function of pressure (b) and absolute salinity (S) (c). Mean profiles (solid lines) and standard deviations (shading) are calculated in density space and sorted into pressure space (as in Dutrieux et al., 2014) before being smoothed with a 5 dbar rolling mean. Water masses discussed in the main text (modified Circumpolar Deep Water, mCDW, and Winter Water, WW) are labelled. Potential density (black contours), the freezing line (thick black line), and an example Gade line indicative of mixing between mCDW and glacial meltwater (dashed black line) are shown for reference in (c). (d) Timeseries of γ, a bulk indicator of stratification strength calculated as the potential energy required to homogenize profiles between 5 and 750 dbars (circles), and the absolute depth of the mCDW layer $\mathrm{AD}_{\mathrm{mCDW}}$, a proxy for the thermocline depth developed by Kim et al. (2021) (crosses) (details in Supporting Information S1). $\mathrm{AD}_{\mathrm{mCDW}}$ and γ values are offset on the time axis for clarity. Variables required for the calculation of $\mathrm{AD}_{\mathrm{mCDW}}$ were not obtained for 2006. Observations were collected in the austral summer between December (previous year) and March (listed year).

2 Methods

2.1 Ice front overturning model

Motivated by observational evidence that the ice front thermocline depth is tied to basal melt rates (Jenkins et al., 2018) and that barotropic heat transport is blocked at the ice shelf front (Wåhlin et al., 2020), we present a purely baroclinic model for heat transport to ice shelves reminiscent of simple models for the global overturning (Walin, 1982; Gnanadesikan, 1999). This baroclinic model represents the shoreward transport of warm mCDW and export of cool surface water masses, including WW and glacially modified CDW, within Amundsen Sea glacially carved troughs (e.g. Webber et al., 2019). This exchange is facilitated by water mass transformation, which may occur within the ice shelf cavity or the ASP. Transformations are modeled in a small region proximate to the ice shelf front, isolating the effect of coastal forcing from shelf-break processes.

Key model components are illustrated in Figure 2. Warm mCDW and overlying thermocline waters are represented as boxes within the small region at the ice shelf front where winter polynya activity is concentrated (50 km meridional, 55 km zonal extent to match the width of the Dotson Ice Shelf). The inflow of warm mCDW, Ψ_{in}, is prescribed to represent remote wind-driven variations in shoreward mCDW transport. This mCDW then transforms into offshore flowing thermocline waters via two pathways: by melting glacial ice and mixing with the resultant meltwater in the ice shelf cavity (Ψ_{ice}) or by mixing with overlying waters (Ψ_{P}) (Figure 2a,b). Assuming negligible volume input from meltwater, the steady state transports balance,

$$\Psi_{\mathrm{in}} = \Psi_{\mathrm{ice}} + \Psi_{\mathrm{P}}. \tag{1}$$

The partitioning of mCDW transformation into Ψ_{ice} and Ψ_{P} is set by the thickness and relative buoyancy (i.e. stratification) of the mCDW and surface boxes. As illustrated in Figure 2c, the thermocline depth (h) and the thickness of the underlying mCDW layer (h_{mCDW}) evolve according to,

$$\frac{\mathrm{d}h}{\mathrm{d}t} = \frac{1}{L}\Big[\Psi_{\mathrm{ice}} + \Psi_{\mathrm{P}} - \Psi_{\mathrm{in}}\Big], \tag{2}$$

$$h_{\mathrm{mCDW}} = H - h, \tag{3}$$

where L is the meridional model extent and H is the ice front water column thickness (taken as 700 m). Ψ terms are converted from thickness fluxes to volume transports (1 Sv $= 10^6$ m^3 s^{-1}) via the model zonal extent. The buoyancy of the mCDW layer (b_{mCDW}) is kept constant, a choice justified by the minimal variability in mCDW density in observations (Figure 1c). We set

$$b_{\mathrm{mCDW}} = 0, \tag{4}$$

referencing our system to the buoyancy of the mCDW layer, such that the buoyancy differential between mCDW and thermocline waters, a metric for the ice front stratification strength, is $\Delta b = b - b_{\mathrm{mCDW}} = b$ where b is the buoyancy of thermocline waters. The stratification strength (Δb) then evolves according to the divergence of buoyancy fluxes from the thermocline (Figure 2c),

$$\frac{\mathrm{d}\Delta b}{\mathrm{d}t} = \frac{1}{L}\Big[(vb)_{\mathrm{in}} - (vb)_{\mathrm{out}}\Big] + \frac{1}{h}\Big[(wb)_{\mathrm{in}} - (wb)_{\mathrm{out}}\Big] \tag{5}$$

where,

$$(vb)_{\mathrm{in}} = \frac{\Psi_{\mathrm{ice}}\Delta b_{\mathrm{melt}}}{h}, \quad \text{and} \tag{6}$$

$$(vb)_{\mathrm{out}} = \frac{\Psi_{\mathrm{in}}\Delta b}{h}. \tag{7}$$

Δb_{melt} is the buoyancy of waters transformed by mixing with ice shelf meltwater, relative to b_{mCDW}, which we determine from hydrography to be 6.7×10^{-3} m s^{-2} (lightest waters in Figure 1c). The vertical buoyancy budget comprises a prescribed surface buoyancy flux due to net sea-ice formation in the polynya,

$$(wb)_{\mathrm{out}} = -F_{\mathrm{surf}} \tag{8}$$

(negative F_{surf} values lower surface ocean buoyancy) and buoyancy loss to the underlying mCDW layer due to mixing ($(wb)_{\mathrm{in}}$). We parameterize the latter as an advection-diffusion balance of buoyancy (e.g. Munk, 1966) which simplifies to

$$(wb)_{\mathrm{in}} = \frac{\Psi_{\mathrm{P}} b_{\mathrm{mCDW}}}{L} - \frac{\kappa_{\mathrm{P}}(b - b_{\mathrm{mCDW}})}{h} = -\frac{\kappa_{\mathrm{P}}\Delta b}{h}. \tag{9}$$

In (9) we select h as the most appropriate length-scale controlling vertical buoyancy transfer, since a thicker surface layer poses greater resistance to entrainment at its lower boundary when the primary energy source driving mixing is input at the surface.

The form of the polynya diffusivity term in (9), κ_{P}, is central to the feedbacks described in this study. Simply put, κ_{P} is a smoothed step function that transitions from a small diffusive end member κ_{diff} when the thermocline is buoyant to a large convective end member κ_{conv} when the thermocline approaches the density of the underlying mCDW. The effect is analogous to rapid transitions to vertical homogeneity triggered

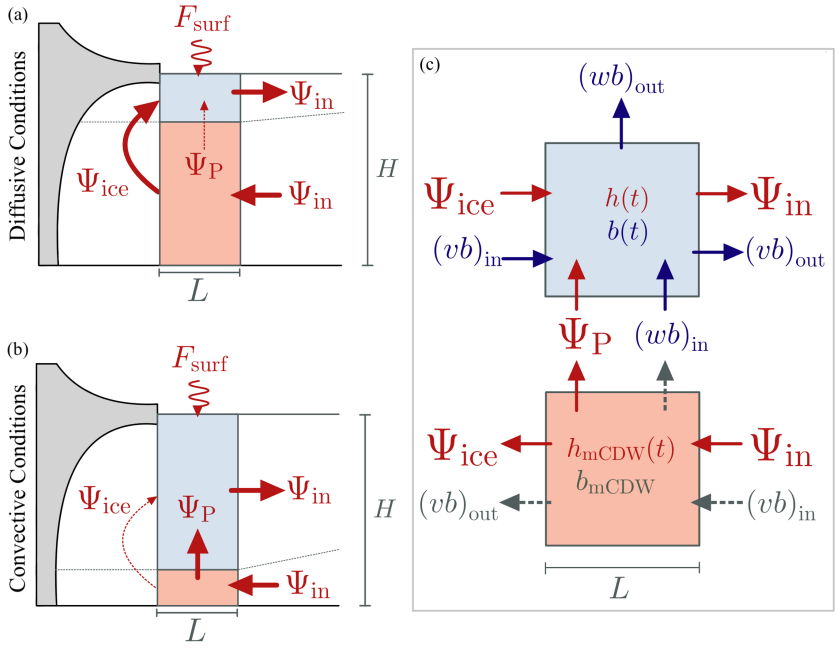

Figure 2. Schematic illustration of the ice front overturning model under (a) diffusive ($\kappa_{\mathrm{P}} \rightarrow \kappa_{\mathrm{diff}}$) and (b) convective ($\kappa_{\mathrm{P}} \rightarrow \kappa_{\mathrm{conv}}$) conditions. The thermocline and modified Circumpolar Deep Water (mCDW) layers are shaded blue and red respectively, and the ice shelf is shaded grey. Thick and dashed red arrows show the primary and secondary transformation pathways associated with each state. Thickness and buoyancy fluxes ($\Psi_{\mathrm{in}}, \Psi_{\mathrm{ice}}, \Psi_{\mathrm{P}}$ and F_{surf}) are indicated. (c) Schematic of the thickness and buoyancy budgets of the thermocline (upper; thickness and buoyancy evolved explicitly) and mCDW (lower; thickness evolved implicitly, buoyancy held constant) layers. The implied buoyancy budget of the mCDW layer is shown in grey, however b_{mCDW} does not evolve.

by static instability in simple models of open ocean polynyas (Martinson et al., 1981; Boot et al., 2021). Functionally, we define κ_{P} as,

$$\kappa_{\mathrm{P}}(\Delta b) = \frac{\kappa_{\mathrm{conv}} - \kappa_{\mathrm{diff}}}{2}\Big(1 - \tanh\big(\phi(\Delta b - \Delta b_{\mathrm{crit}})\big)\Big) + \kappa_{\mathrm{diff}}, \tag{10}$$

where κ_{conv} (10^{-2} m s^{-2}) and κ_{diff} (10^{-4} m s^{-2}, taken from summertime Pine Island Ice Front observations Garabato et al., 2017)(10^{-4} m s^{-2}) are vertical diffusivities, Δb_{crit} ($5{\times}10^{-4}$ m s^{-2}) is a small stratification strength at which turbulent convection onsets, and ϕ ($5{\times}10^{4}$) is a parameter determining the steepness of the onset of convection. Our results are not sensitive to reasonable perturbations of the parameters.

The polynya mass transport term Ψ_{P} is constructed to be consistent with (9),

$$\Psi_{\mathrm{P}} = -\frac{\kappa_{\mathrm{P}} L}{h}. \tag{11}$$

Finally, the ice cavity overturning Ψ_{ice} is taken to be linearly proportional to the mCDW thickness,

$$\Psi_{\mathrm{ice}} = \alpha h_{\mathrm{mCDW}} = \alpha(H - h), \tag{12}$$

where α ($2.1{\times}10^{-3}$ m s^{-1}) is diagnosed from the WAIS 1080 regional simulation (see §2.2 and Supporting Information S2).

To summarize, the ice front overturning model is described by the following coupled differential equations for the thermocline depth (h) and stratification strength (Δb),

$$\frac{\mathrm{d}h}{\mathrm{d}t} = \frac{1}{L}\Big[\alpha(H - h) - \frac{\kappa_{\mathrm{P}} L}{h} - \Psi_{\mathrm{in}}\Big], \tag{13}$$

$$\frac{\mathrm{d}\Delta b}{\mathrm{d}t} = \frac{1}{Lh}\Big[\alpha(H - h)\Delta b_{\mathrm{melt}} - \Psi_{\mathrm{in}}\Delta b\Big] + \frac{1}{h^2}\Big[F_{\mathrm{surf}} h - \kappa_{\mathrm{P}}\Delta b\Big]. \tag{14}$$

All parameter values except the diffusivity κ_{P} are diagnosed from observations or WAIS 1080 (§2.2), and Ψ_{in} and F_{surf} are prescribed forcings representing the supply of mCDW (a remote forcing) and polynya surface buoyancy fluxes from sea ice(a local forcing).

2.2 Regional general circulation model

In addition to the ice front overturning model, we utilize monthly mean output from WAIS 1080, a high-resolution ($\sim$ 3 km horizontal spacing) regional numerical ocean model, based on the Massachusetts Institute of Technology general circulation model (MITgcm), that represents the tip of the Antarctic Peninsula to the western edge of the Amundsen Sea (Flexas et al., 2022). The model is forced at the surface by the European Centre for Medium-Range Weather Forecasts (ECMWF) reanalysis version 5 (ERA5; Hersbach et al., 2020) and integrated from 1992 to 2019. WAIS 1080 explicitly represents freezing and melting within ice shelf cavities of a fixed shape, making it suited to the study of ocean ice-shelf interactions at relatively short timescales. We use the control simulation from Flexas et al. (2022), who provide additional model details, to constrain the values of parameters (α) and forcings (F_{surf}, Ψ_{in}) of the ice front overturning model that are difficult to obtain directly from observations. Details of how α, F_{surf}, and Ψ_{in} values are obtained from WAIS 1080 are provided in Supporting Information S2.

3 Results

3.1 Steady state model behavior

Equilibrated solutions of the ice front overturning model map a hysteresis loop for the thermocline depth in response to varying surface buoyancy forcing (F_{surf}) when the supply of mCDW from the shelf-break (Ψ_{in}) is held fixed (Figure 3a). Thus, warm and

cold regimes can be realized with the same mCDW supply. This hysteresis loop is enabled by a positive feedback between the depth of the ice front thermocline and the stratification of the ice front water column, the physics of which are parameterized in our vertical diffusivity term κ_{P}. A shallow ice front thermocline, equivalent to a thick mCDW layer, supports high melt rates within the cavity. The ensuing meltwater provides an additional buoyancy input to the thermocline that suppresses convection and reinforces the shallow thermocline position (upper "branch" of the hysteresis loop, Figure 3a). By contrast, a deep ice front thermocline, equivalent to a thin mCDW layer, is associated with a weaker ice shelf melt rate and a reduced input of buoyant meltwater to the WW layer, comparatively preconditioning the water column for convection and reinforcing the deep thermocline position (lower "branch", Figure 3a). This feedback produces bistable "diffusive" ($\kappa_{\mathrm{P}} = \kappa_{\mathrm{diff}}$, thick mCDW) and "convective" ($\kappa_{\mathrm{P}} = \kappa_{\mathrm{conv}}$, thin mCDW) steady states for a fixed supply of mCDW associated with an $\sim$ (400 m) thermocline depth differential. In this idealized model, most convective steady states are unstably stratified ($b_{\mathrm{WW}} < 0$, i.e. $b_{\mathrm{WW}} < b_{\mathrm{mCDW}}$) as they arise when strong negative buoyancy forcing is continuously applied. These bistable states have comparable mCDW depths to the ob-

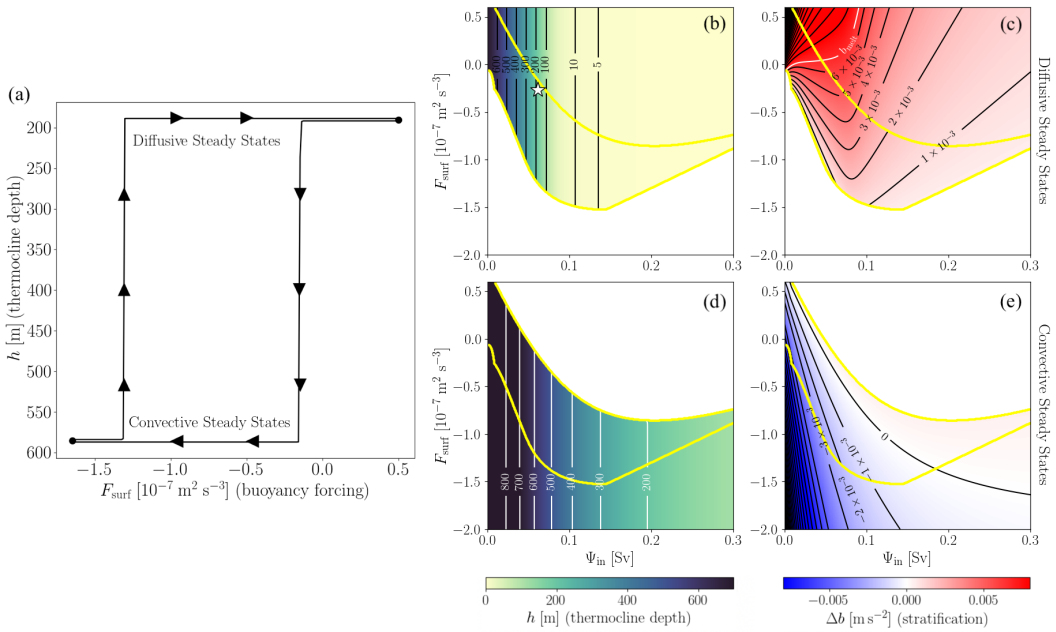

Figure 3. (a) Dependence of the model steady state on F_{surf} when Ψ_{in} is held fixed at the mean WAIS 1080 value (0.06 Sv). The model is evolved to steady state after incrementally increasing and decreasing values of F_{surf} (direction indicated by arrows) spanning the range simulated in WAIS 1080. The forward and reverse pathways are offset to aid visualization. Text inset identifies solutions associated with $\kappa_{\mathrm{P}} = \kappa_{\mathrm{conv}}$ ("convective steady states") and $\kappa_{\mathrm{P}} = \kappa_{\mathrm{diff}}$ ("diffusive steady states"). (b-e) Plots showing equilibrated h (b,d) and Δb (c,e) values associated with diffusive steady states (b,c) and convective steady states (d,e) for a range of Ψ_{in} and F_{surf} forcing values. Regions of each phase space left white do not support steady states with the relevant κ_{P} value. Yellow contours outline the parameter space able to support both diffusive and convective steady states. The white star in (b) shows the time mean WAIS 1080 forcing. Convective steady states to with $h > 700$ m (depth of the water column) are not physical, but are shown here since transient forcing in this region is permissible.

served warm and cool phases (Figure 1d), although observed cool phases, which are sampled exclusively during summer months, are stably stratified.

Bistability occurs over a large portion of the explored forcing space (yellow contour in Figure 3b-e), which spans realistic ranges of F_{surf} and Ψ_{in} (monthly mean values span -1.7×10^{-7} to 0.5×10^{-7} m^2 s^{-3} and 0 to 0.3 Sv in WAIS 1080). Forcing combinations that support only one steady state solution are referred to as monostable. Figure 3b-e suggests variations in both F_{surf} (vertical paths in Figure 3b-e) and Ψ_{in} (horizontal paths) can generate hysteresis by shifting the system from one monostable region to the other via the bistable region. Whilst Figure 3 displays numerically equilibrated model output, a benefit of this model's simplicity is that it permits analytical solutions for end member cases and easy exploration of parameter space (Supporting Information S3). Overall, model behavior is not qualitatively sensitive to reasonable parameter perturbations; a summary of our sensitivity assessment appears in Table S1.

3.2 Transient model behavior

The presence of bistability in this simple model poses an alternate explanation for the decadal scale $\sim$ 400 m thermocline depth variations observed at the Dotson Ice Front. The observed variability could, as previously implied, be a low frequency response to low frequency variations in the supply of mCDW to the ice front. Alternatively, our simple model suggests that transient perturbations of either mCDW supply or coastal surface buoyancy fluxes could trigger transitions between self-reinforcing deep and shallow thermocline states, perhaps explaining the large amplitude and persistent nature of the observed cool and warm phases. This possibility is tested with transiently forced experiments.

The ice front overturning model is initialized with either weak or strong stratification and forced with WAIS 1080 climatological mean F_{surf} and Ψ_{in} values until annual patterns of ice front stratification (Δb) and thermocline depth (h) equilibrate. The WAIS 1080 climatology lies sufficiently within the bistable forcing region (yellow shaded region in Figure 4a,b) to support temporally varying solutions that persist in their initial diffusivity regime. These equilibrated simulations are then transiently forced with perturbed climatologies to prompt regime transitions that persist when the forcing returns to the original pattern. Two winter perturbations are constructed by decreasing the May-September F_{surf} or Ψ_{in} forcing by a constant offset, and two summer perturbations are constructed by increasing the December-April F_{surf} or Ψ_{in} forcing by a constant offset. Winter and summer perturbations are then tested for their ability to drive transitions from the diffusive to the convective regime and vice versa. Seasonal perturbations are chosen based on the strong seasonality of F_{surf}; we also use a seasonal perturbation for Ψ_{in} experiments for consistency, although Ψ_{in} has a more complex annual pattern (Figure 4b inset).

Figure 4a,b show the smallest amplitude winter and summer offsets that trigger regime shifts within two consecutive years of perturbed forcing. When regime transitions are simulated (Figure 4c,e,f), lags between the thermocline response and stratification response align with observations. In agreement with the observed transition from a warm phase to a cool phase between 2009 and 2012 (Figure 1d), thermocline depth anomalies lag buoyancy anomalies during modeled transitions to convective conditions (Figure 4c). The shoaled thermocline observed in 2018 may represent a transition to warm phase conditions with the opposite lag, thermocline shoaling preceding stratification strengthening. If so, the simulated lags between thermocline depth anomalies and buoyancy anomalies in both Ψ_{in} and F_{surf}-driven transitions to diffusive conditions (Figure 4d,e) are also consistent with observations.

In addition to capturing the nature of observed transitions between warm and cool phases at the Dotson Ice Front, our idealized model anticipates the shallow bias and di-

minished variability of the ice front thermocline depth in WAIS 1080 (0°C isotherm depth ranges from 440-820 m in observations and only 255-420 m in WAIS 1080). When the ice front overturning model is forced with the full WAIS 1080 1992-2019 timeseries of F_{surf} and Ψ_{in}, rather than climatological values, simulations initialized with convective conditions rapidly transition to diffusive conditions and remain there (Figure S5), consistent with WAIS 1080 failing to capture convective events. In general, transitions to convective states required larger deviations from the WAIS 1080 forcing than transitions to diffusive states. Significantly stronger negative F_{surf} values than those simulated in WAIS 1080 were needed to generate a regime shift within a single year (minimum winter values of -3×10^{-7} m^2 s^{-3} compared to minimum WAIS 1080 forcing of -1.7×10^{-7} m^2 s^{-3}), thus our choice to present results of two-year perturbations in Figure 4. ERA5 has been shown to underestimate near-surface wind speeds along the Antarctic coastline (Caton Harrison et al., 2022) and this may induce an underestimation of winter F_{surf} minima in WAIS 1080, alternatively, WAIS 1080 and our idealized model may exaggerate the barrier to convection.

Reductions in Ψ_{in}, whether transient (Figure 4d) or more sustained (Figure S6), do not trigger transitions to convective conditions for any physical choice of offset (i.e. enforcing $\Psi_{\text{in}} > 0$). Such regime shifts are not supported as reducing Ψ_{in} initially strengthens ice front stratification in our simulations. This anticorrelation between thermocline depth and stratification when Ψ_{in} is reduced is not supported by observations or WAIS 1080, however, and may reflect the simplicity of our model. These experiments affirm the possibility that polynya forcing can drive realistic transitions to cool phases, but do not negate the possibility that variable mCDW supply could also drive such transitions. Both forcings appear able to drive realistic transitions to warm conditions.

4 Discussion and Outlook

This study intentionally targets a simplified representation of West Antarctic coastal ocean dynamics to highlight mechanistic links between surface forcing, interior mixing, thermocline depth variations, and overturning pathways on the West Antarctic continental shelf. The key result is the identification of positive feedbacks that are independent of the supply of mCDW from the continental shelf break. These dynamics involve interactions between basal ice shelf melt rates and thermocline stratification at the ice shelf front, and provide a plausible explanation for the amplitude and duration of multi-year warm and cool phases observed, for example, at the Dotson Ice Front. The modeled thermocline variability tracks the strength of convection in the adjacent coastal polynya and successfully reproduces observed stratification changes, not previously identified, associated with transitions between the warm and cool phases. These low frequency variations in convection may arise either from a variable mCDW supply from the continental shelf break (a remote forcing), or from surface buoyancy fluxes within the polynya (a local forcing). Since future trends in mCDW supply from the shelf-break and sea-ice production in coastal polynyas may not align, understanding the relative importance of these forcings is important for projecting future melt. Critically, the positive feedback identified here cannot be represented in complex ocean models that apply fixed meltwater inputs. This study motivates analysis in models that simulate basal melt within cavities. As a first step on this path, we show that the the idealized model predicts the shallow, steady bias of the Dotson Ice Front thermocline in the WAIS 1080 model based on its forcing, demonstrating the power of using a combination of idealized and complex models to characterize model biases. Additionally, our results point to ice front stratification as a key target diagnostic for simulations of West Antarctic ocean-forced ice shelf melt. Finally, this study emphasizes the importance of water mass transformation, both over the shelf and in ice shelf cavities, as a key process that links shelf-break and coastal processes through closure of the shelf overturning circulation.

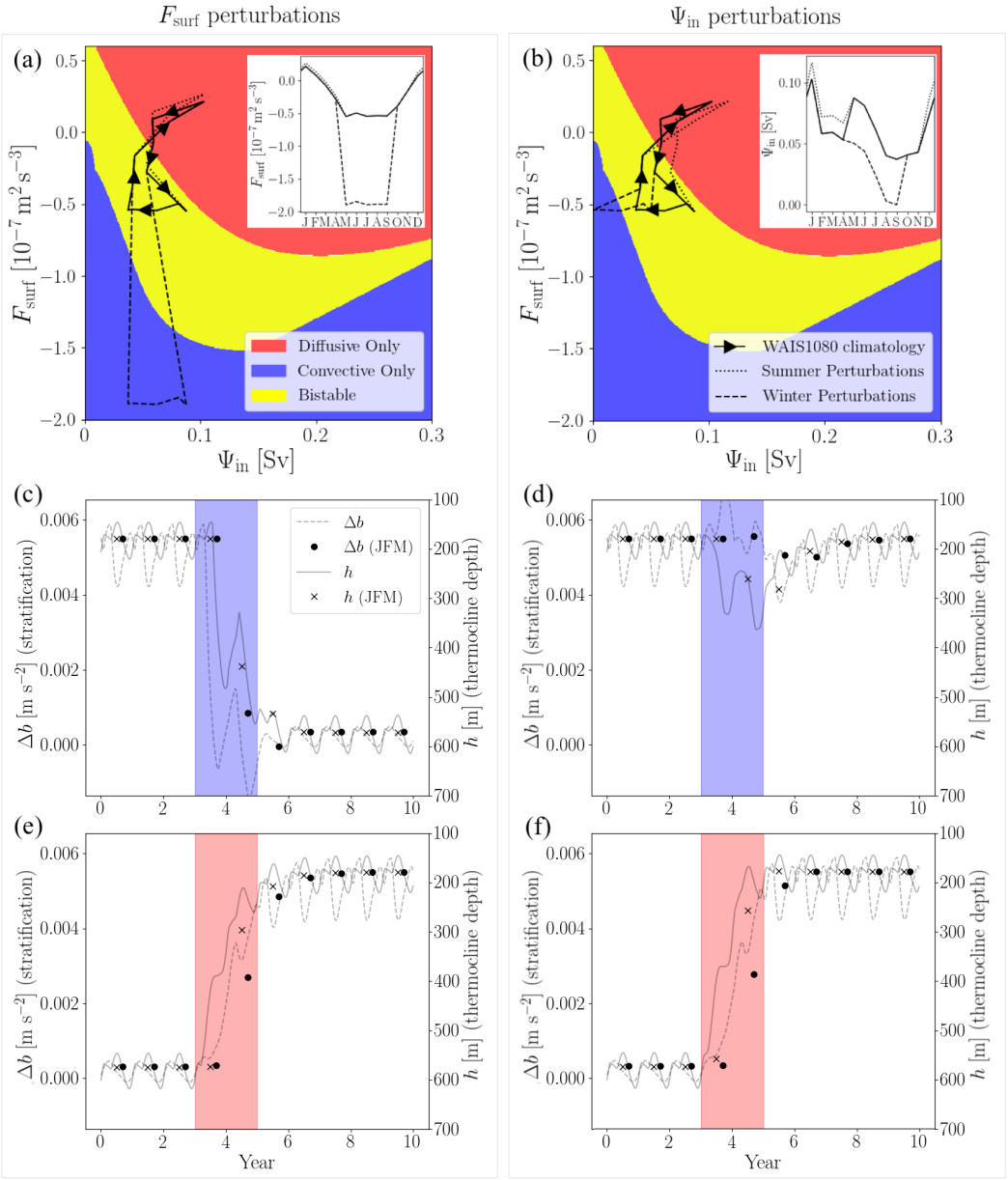

Figure 4. (a, b) The forcing parameter space partitioned into regions supporting only one steady state solution (diffusive in red; convective in blue) and both solutions (bistability in yellow. Climatological mean F_{surf} and Ψ_{in} values from the WAIS 1080 simulation are shown within this forcing space (solid black lines) with arrows indicating the progression of an annual cycle. Winter perturbed forcings (dashed lines) and summer perturbed forcings (dotted lines) are indicated within the forcing space for F_{surf} experiments (a) and Ψ_{in} experiments (b). Forcing climatologies are shown as a function of time in inset panels for clarity. (c-f) Full time series of h (solid grey lines) and Δb (dashed grey lines) alongside January-March mean values (black crosses and circles, respectively) from transient forcing experiments described in the main text. Shaded regions indicate the perturbation period (years 4 and 5) and whether a winter (blue; c,d) or summer (red; e,f) perturbation was prescribed.

The idealized representation of coastal dynamics in this study neglects certain processes that merit discussion. The most notable simplification is that WW, meltwater modified CDW, and other surface waters are combined in a single box. As a result, the spatial structure of glacial meltwater plumes exiting the cavity (e.g. Garabato et al., 2017; Zheng et al., 2021) and exiting the model domain are omitted, and buoyancy from meltwater is uniformly distributed above the thermocline. This simplification may lead to spurious stratification strengthening in response to reductions in mCDW supply (Figure 4d), as unresolved structures may remove meltwaters from the ice shelf front more rapidly than our model suggests. The truncated vertical structure of our model also leads to unrealistic year-round convection during cool phases in transiently forced simulations (Figure 4). In the real ocean, positive F_{surf} forcing during summer months may halt convection by stratifying a small fraction of the upper water column whilst leaving the deep thermocline position intact. In our model, positive buoyancy fluxes are distributed over the full thermocline depth, presenting an exaggerated barrier to restratification. Consequently, the water column convects year-round rather than being preconditioned for the annual recurrence of convection. Another noteworthy simplification is that, since Ψ_{in} and F_{surf} are prescribed, we neglect feedbacks that influence their magnitude. Shoreward mCDW transport in the Amundsen Sea may decrease (Moorman et al., 2020; Beadling et al., 2022) or increase (Si et al., 2023) in response to coastal freshening, and coastal sea-ice formation rates may likewise be sensitive to coastal freshening by meltwater. Further work is necessary to synthesize these complex responses to changing melt rates and simple models, such as the one presented here, may be useful tools in this effort. The ability for our idealized model to capture key features of observed Amundsen Sea mCDW variability despite these simplifications speaks to the importance of ice front thermocline stratification strength to ocean-driven glacial melt variability on decadal timescales.

This work builds on regional modeling (St-Laurent et al., 2015; Caillet et al., 2022; Naughten et al., 2022), idealized modeling (Petty et al., 2013; Silvano et al., 2018), and observational evidence (Webber et al., 2017) indicating coastal buoyancy forcing can modulate ocean heat availability at West Antarctic ice shelves. In agreement with our findings, anomalously strong coastal surface buoyancy fluxes can explain the 2011-2013 cool period observed at the Pine Island Ice Front (St-Laurent et al., 2015; Webber et al., 2017). At longer timescales, simulated deep coastal warming trends have been associated with centennial scale reductions in coastal convection (Naughten et al., 2022), and simulated transitions between more dramatic cool and warm Amundsen shelf states closely track surface buoyancy forcing changes (Caillet et al., 2022). Idealized models, on the other hand, have primarily been used to assess the Amundsen Sea mean state, with bulk mixed layer models indicating a leading role for buoyancy fluxes in setting the shallow winter mixed layer depths typical of the West Antarctic shelf relative to other Antarctic regions (Petty et al., 2013; Silvano et al., 2018). Whilst Amundsen Sea variability at interannual and longer timescales has not been targeted with idealized models, there is precedent elsewhere. For example, conceptual models have been used to interrogate bistable low and high melt states of the Filchner-Ronne Ice Shelf enabled by coastal buoyancy feedbacks analogous to those identified here (Hazel & Stewart, 2020). Our approach incorporates the consideration of buoyancy central to these results into a "thermocline model" framework based on closing watermass transformation pathways, a framework originally applied to the global overturning circulation (e.g. Gnanadesikan, 1999; Marshall & Zanna, 2014; Thompson et al., 2019).

We take away two important lessons for future studies of warm West Antarctic shelf seas. Firstly, the dynamics that govern the exposure of ice shelves to ocean heat must account not only for variability in mCDW supply, but also mCDW consumption or transformation, with the latter having received significantly less attention. Secondly, we cannot neglect the dynamical effects of meltwater in a salinity stratified system; ongoing observational monitoring and accurate simulation of ice front stratification strength should be prioritized.

Open Research Section

Data and code required to reproduce all figures in the main text and Supporting Information provided at `https://doi.org/10.5281/zenodo.7987113`. A binder environment (see `https://mybinder.org/` for details) has been constructed so that readers can open, edit, and execute all code from a browser (click "launch binder" button on the GitHub repository home page linked to the listed doi). Editing within the binder environment will not alter the original file, so readers should feel free to manipulate provided code.

Acknowledgments

RM acknowledges the funding support of the General Sir John Monash Foundation. AT acknowledges support from NSF grants OPP-1644172 and OCE-2023259. EW acknowledges support from Caltech's Terrestrial Hazard Observations and Reporting Center. We thank Michael Schodlock and Mar Flexas for their assistance in accessing and utilizing WAIS 1080 output. We thank Channing Prend for his helpful comments on the initial manuscript. We also thank Kevin Speer and Alessandro Silvano for helpful conversations. Finally, we acknowledge valuable work performed in the collection, collation and open access publishing of shipborne observational data by the Marine Geoscience Data System (MGDS), the Korean Polar Data Center (KPDC), and the authors of Jenkins et al. (2018).

References

Adusumilli, S., Fricker, H. A., Medley, B., Padman, L., & Siegfried, M. R. (2020). Interannual variations in meltwater input to the southern ocean from antarctic ice shelves. *Nature geoscience*, *13*(9), 616–620.

Assmann, K. M., Jenkins, A., Shoosmith, D. R., Walker, D. P., Jacobs, S. S., & Nicholls, K. W. (2013). Variability of circumpolar deep water transport onto the Amundsen Sea Continental shelf through a shelf break trough. *Journal of Geophysical Research: Oceans*, *118*(12), 6603–6620. doi: 10.1002/2013JC008871

Beadling, R., Krasting, J., Griffies, S., Hurlin, W., Bronselaer, B., Russell, J., ... Winton, M. (2022). Importance of the antarctic slope current in the southern ocean response to ice sheet melt and wind stress change. *Journal of Geophysical Research: Oceans*, *127*(5), e2021JC017608.

Boot, D., Van Westen, R. M., & Dijkstra, H. A. (2021, feb). Multidecadal polynya formation in a conceptual (box) model. *Ocean Science*, *17*(1), 335–350. doi: 10.5194/os-17-335-2021

Caillet, J., Jourdain, N. C., Mathiot, P., Hellmer, H. H., & Mouginot, J. (2022). Drivers and reversibility of abrupt ocean state transitions in the amundsen sea, antarctica. *Journal of Geophysical Research: Oceans*, e2022JC018929.

Caton Harrison, T., Biri, S., Bracegirdle, T. J., King, J. C., Kent, E. C., Vignon, É., & Turner, J. (2022). Reanalysis representation of low-level winds in the antarctic near-coastal region. *Weather and Climate Dynamics*, *3*(4), 1415–1437.

Dotto, T. S., Garabato, A. C., Bacon, S., Holland, P. R., Kimura, S., Firing, Y. L., ... Jenkins, A. (2019). Wind-driven processes controlling oceanic heat delivery to the amundsen sea, antarctica. *Journal of Physical Oceanography*, *49*(11), 2829–2849. doi: 10.1175/JPO-D-19-0064.1

Dotto, T. S., Garabato, A. C. N., Wåhlin, A. K., Bacon, S., Holland, P. R., Kimura, S., ... Jenkins, A. (2020). Control of the Oceanic Heat Content of the Getz-Dotson Trough, Antarctica, by the Amundsen Sea Low. *Journal of Geophysical Research: Oceans*, *125*(8), e2020JC016113. doi: 10.1029/2020JC016113

Dutrieux, P., De Rydt, J., Jenkins, A., Holland, P. R., Ha, H. K., Lee, S. H., ... Schröder, M. (2014). Strong sensitivity of Pine Island ice-shelf melting to cli-

matic variability. *Science*, *343*(6167), 174–178. doi: 10.1126/science.1244341

Fetterer, F., & Stewart., J. S. (2020). *U.S. National Ice Center Arctic and Antarctic Sea Ice Concentration and Climatologies in Gridded Format, Version 1.* National Snow and Ice Data Center. Retrieved from `https://nsidc.org/data/g10033/versions/1` doi: 10.7265/46cc-3952

Flexas, M. M., Thompson, A. F., Schodlok, M. P., Zhang, H., & Speer, K. (2022). Antarctic peninsula warming triggers enhanced basal melt rates throughout west antarctica. *Science Advances*, *8*(31), eabj9134.

Fretwell, P., Pritchard, H. D., Vaughan, D. G., Bamber, J. L., Barrand, N. E., Bell, R., ... others (2013). Bedmap2: improved ice bed, surface and thickness datasets for antarctica. *The cryosphere*, *7*(1), 375–393.

Fürst, J. J., Durand, G., Gillet-Chaulet, F., Tavard, L., Rankl, M., Braun, M., & Gagliardini, O. (2016). The safety band of Antarctic ice shelves. *Nature Climate Change*, *6*(5), 479–482. doi: 10.1038/NCLIMATE2912

Garabato, A. C. N., Forryan, A., Dutrieux, P., Brannigan, L., Biddle, L. C., Heywood, K. J., ... Kimura, S. (2017). Vigorous lateral export of the meltwater outflow from beneath an antarctic ice shelf. *Nature*, *542*(7640), 219–222.

Gnanadesikan, A. (1999). A simple predictive model for the structure of the oceanic pycnocline. *Science*, *283*(5410), 2077–2079. doi: 10.1126/science.283.5410.2077

Hazel, J. E., & Stewart, A. L. (2020, apr). Bistability of the Filchner-Ronne Ice Shelf Cavity Circulation and Basal Melt. *Journal of Geophysical Research: Oceans*, *125*(4), e2019JC015848. doi: 10.1029/2019JC015848

Hersbach, H., Bell, B., Berrisford, P., Hirahara, S., Horányi, A., Muñoz-Sabater, J., ... others (2020). The era5 global reanalysis. *Quarterly Journal of the Royal Meteorological Society*, *146*(730), 1999–2049.

IMBIE Team. (2018). Mass balance of the Antarctic Ice Sheet from 1992 to 2017. *Nature 2018 558:7709*, *558*(7709), 219–222. doi: 10.1038/s41586-018-0179-y

Jenkins, A., Dutrieux, P., Jacobs, S., Steig, E. J., Gudmundsson, G. H., Smith, J., & Heywood, K. J. (2016). Decadal Ocean Forcing and Antarctic Ice Sheet Response: LESSONS FROM THE AMUNDSEN SEA. *Oceanography*, *29*(4), 106–117.

Jenkins, A., Shoosmith, D., Dutrieux, P., Jacobs, S., Kim, T. W., Lee, S. H., ... Stammerjohn, S. (2018). West Antarctic Ice Sheet retreat in the Amundsen Sea driven by decadal oceanic variability. *Nature Geoscience*, *11*(10), 733–738. doi: 10.1038/s41561-018-0207-4

Kim, T. W., Ha, H. K., Wåhlin, A. K., Lee, S. H., Kim, C. S., Lee, J. H., & Cho, Y. K. (2017, jan). Is Ekman pumping responsible for the seasonal variation of warm circumpolar deep water in the Amundsen Sea? *Continental Shelf Research*, *132*, 38–48. doi: 10.1016/j.csr.2016.09.005

Kim, T.-W., Yang, H. W., Dutrieux, P., Wåhlin, A. K., Jenkins, A., Kim, Y. G., ... Cho, Y.-K. (2021). Interannual Variation of Modified Circumpolar Deep Water in the Dotson-Getz Trough, West Antarctica. *Journal of Geophysical Research: Oceans*, *126*(12), e2021JC017491.

Marshall, D. P., & Zanna, L. (2014). A conceptual model of ocean heat uptake under climate change. *Journal of Climate*, *27*(22), 8444–8465.

Martinson, D. G., Killworth, P. D., & Gordon, A. L. (1981). A convective model for the weddell polynya. *Journal of Physical Oceanography*, *11*(4), 466–488.

Moorman, R., Morrison, A. K., & McC. Hogg, A. (2020). Thermal responses to antarctic ice shelf melt in an eddy-rich global ocean–sea ice model. *Journal of Climate*, *33*(15), 6599–6620.

Morlighem, M., Rignot, E., Binder, T., Blankenship, D., Drews, R., Eagles, G., ... Young, D. A. (2020). Deep glacial troughs and stabilizing ridges unveiled beneath the margins of the Antarctic ice sheet. *Nature Geoscience*, *13*(2), 132–137. doi: 10.1038/s41561-019-0510-8

Mouginot, J., Rignot, E., & Scheuchl, B. (2014). Sustained increase in ice discharge from the amundsen sea embayment, west antarctica, from 1973 to 2013. *Geophysical Research Letters*, *41*(5), 1576–1584.

Munk, W. H. (1966). Abyssal recipes. In *Deep sea research and oceanographic abstracts* (Vol. 13, pp. 707–730).

Naughten, K. A., Holland, P. R., Dutrieux, P., Kimura, S., Bett, D. T., & Jenkins, A. (2022). Simulated twentieth-century ocean warming in the amundsen sea, west antarctica. *Geophysical Research Letters*, *49*(5), e2021GL094566.

Paolo, F. S., Fricker, H. A., & Padman, L. (2015). Volume loss from antarctic ice shelves is accelerating. *Science*, *348*(6232), 327–331. doi: 10.1126/science.aaa0940

Petty, A. A., Feltham, D. L., & Holland, P. R. (2013). Impact of atmospheric forcing on antarctic continental shelf water masses. *Journal of Physical Oceanography*, *43*(5), 920–940.

Pritchard, H., Ligtenberg, S. R., Fricker, H. A., Vaughan, D. G., van den Broeke, M. R., & Padman, L. (2012). Antarctic ice-sheet loss driven by basal melting of ice shelves. *Nature*, *484*(7395), 502–505.

Schmidtko, S., Heywood, K. J., Thompson, A. F., & Aoki, S. (2014). Multidecadal warming of antarctic waters. *Science*, *346*(6214), 1227–1231.

Shepherd, A., Wingham, D., & Rignot, E. (2004). Warm ocean is eroding west antarctic ice sheet. *Geophysical Research Letters*, *31*(23).

Si, Y., Stewart, A. L., & Eisenman, I. (2023). Heat transport across the antarctic slope front controlled by cross-slope salinity gradients. *Science Advances*, *9*(18), eadd7049.

Silvano, A., Holland, P. R., Naughten, K. A., Dragomir, O., Dutrieux, P., Jenkins, A., ... others (2022). Baroclinic ocean response to climate forcing regulates decadal variability of ice-shelf melting in the amundsen sea. *Geophysical Research Letters*, *49*(24), e2022GL100646.

Silvano, A., Rintoul, S. R., Peña-Molino, B., Hobbs, W. R., Van Wijk, E., Aoki, S., ... Williams, G. D. (2018, apr). Freshening by glacial meltwater enhances melting of ice shelves and reduces formation of Antarctic Bottom Water. *Science Advances*, *4*(4), eaap9467. doi: 10.1126/sciadv.aap9467

St-Laurent, P., Klinck, J. M., & Dinniman, M. S. (2015). Impact of local winter cooling on the melt of Pine Island Glacier, Antarctica. *Journal of Geophysical Research: Oceans*, *120*(10), 6718–6732. doi: 10.1002/2015JC010709

Thompson, A. F., Hines, S. K., & Adkins, J. F. (2019). A southern ocean mechanism for the interhemispheric coupling and phasing of the bipolar seesaw. *Journal of Climate*, *32*(14), 4347–4365.

Turner, J., Orr, A., Gudmundsson, G. H., Jenkins, A., Bingham, R. G., Hillenbrand, C.-D., & Bracegirdle, T. J. (2017). Atmosphere-ocean-ice interactions in the amundsen sea embayment, west antarctica. *Reviews of Geophysics*, *55*(1), 235–276.

Wåhlin, A. K., Steiger, N., Darelius, E., Assmann, K. M., Glessmer, M. S., Ha, H. K., ... Viboud, S. (2020). Ice front blocking of ocean heat transport to an Antarctic ice shelf. *Nature*, *578*(7796), 568–571. doi: 10.1038/s41586-020-2014-5

Walin, G. (1982). On the relation between sea-surface heat flow and thermal circulation in the ocean. *Tellus*, *34*(2), 187–195.

Walker, D. P., Brandon, M. A., Jenkins, A., Allen, J. T., Dowdeswell, J. A., & Evans, J. (2007). Oceanic heat transport onto the Amundsen Sea shelf through a submarine glacial trough. *Geophysical Research Letters*, *34*(2). doi: 10.1029/2006GL028154

Webber, B. G., Heywood, K. J., Stevens, D. P., & Assmann, K. M. (2019). The impact of overturning and horizontal circulation in pine Island trough on ice shelf melt in the eastern Amundsen Sea. *Journal of Physical Oceanography*,

49(1), 63–83. doi: 10.1175/JPO-D-17-0213.1

Webber, B. G., Heywood, K. J., Stevens, D. P., Dutrieux, P., Abrahamsen, E. P., Jenkins, A., ... Kim, T. W. (2017). Mechanisms driving variability in the ocean forcing of Pine Island Glacier. *Nature Communications*, *8*(1), 1–8. doi: 10.1038/ncomms14507

Zheng, Y., Heywood, K. J., Webber, B. G., Stevens, D. P., Biddle, L. C., Boehme, L., & Loose, B. (2021). Winter seal-based observations reveal glacial meltwater surfacing in the southeastern amundsen sea. *Communications Earth & Environment*, *2*(1), 40.